EXPLORATIVE GRADIENT METHOD FOR HIGH-DIMENSIONAL ACTUATION PARAMETER SPACES

Yiqing Li
School of Mechanical Engineering and Automation
Harbin Institute of Technology, Shenzhen
Shenzhen 518055, China
anne.yiqing.li@outlook.com

Zhigang Yang
Shanghai Automotive Wind Tunnel Center
Tongji University
Shanghai 201804, China
zhigangyang@tongji.edu.cn

Marek Morzyński
Department of Virtual Engineering
Poznań University of Technology
PL 60-965 Poznań, Poland
morzynski@virtual.edu.pl

Bernd R. Noack
School of Mechanical Engineering and Automation
Harbin Institute of Technology, Shenzhen
Shenzhen 518055, China
bernd.noack@hit.edu.cn

ABSTRACT

This paper presents the application of explorative gradient method (EGM) (Li *et al.*, 2022) to three open-loop flow control benchmarks with multiple actuators. The fluidic pinball with three rotating cylinders, the advanced fluidic pinball with six rotating cylinders, and the Ahmed body with seven distributed blowing slots.

The first trial is to minimize the net drag power of the fluidic pinball by three rotating cylinders. The net drag power of the 3-cylinder configuration is reduced by 29%, 52% drag reduction at a price of 23% actuation energy. The configuration is extended further with 3 more cylinders, which ends with 14% net drag reduction. The 35° slanted Ahmed body employing distributed steady blowing is included as a more practical example. 17% drag reduction is achieved in this 10-dimensional design space.

The boat tailing as an effective strategy is verified in design spaces with the dimension ranging from 3 to 10. EGM shows an advantage of tackling high-dimensional optimization for active flow control by reducing the simulation cost from $O(1000)$ to $O(100)$.

INTRODUCTION

Actuators and sensors become increasingly cheaper, powerful and reliable. This trend makes active flow control of increasing interest to industry. In addition, distributed actuation can give rise to performance benefits over single actuator solutions. Here, we focus on the simple case of open-loop control with steady or periodic operation of multiple actuators. Even for this simple case, the optimization of actuation constitutes an algorithmic challenge. Often the budget for optimization is limited to $O(100)$ high fidelity simulations, like direct numerical simulations (DNS) or large-eddy simulations (LES) or $O(100)$ water tunnel experiments, or $O(1000)$ Reynolds Averaged Navier-Stokes (RANS) simulations, or a similar amount of wind-tunnel experiments. Moreover, the optimization may need to be performed for multiple operating conditions. The efficient optimizers are thus of large practical importance (Blanchard & Sapsis, 2021).

In this paper, this challenge is addressed by a new optimizer, called explorative gradient method (EGM) (Li *et al.*, 2022). EGM alternatively performs one exploitive downhill simplex step and an explorative Latin hypercube sampling iteration. Thus, the convergence rate of a gradient based method is guaranteed while, at the same time, better minima are explored. EGM is found to be two times faster than the Genetic algorithm (GA) on an analytical function. When applied to the fuel distribution optimization across the fuel lines, EGM only spends a quarter of the cost by the Evolutionary algorithm (EA) (Reumschüssel *et al.*, 2022).

The fluidic pinball (Ishar *et al.*, 2019; Deng *et al.*, 2020) includes three equal, parallel, equidistantly placed cylinders. The a two-dimensional flow can be changed by the three rotation velocities of the cylinders. The dynamics is rich in nonlinear behaviour, yet geometrically simple and physically interpretable. With suitable rotation of the cylinders many known wake stabilizing and drag-reducing mechanisms can be realized: (1) Coanda actuation (Geropp, 1995), (2) circulation control (Magnus effect), (3) base bleed (Wood, 1964), (4) high-frequency forcing (Thiria *et al.*, 2006), (5) low-frequency forcing (Glezer *et al.*, 2005) and (6) phasor control (Protas, 2004). In this study, constant rotations are optimized for net drag power reduction accounting for the actuation energy. This search space implies the first three mechanisms.

This study also targets the drag reduction of the low-drag Ahmed body with rear slant angle of 35 degrees. This Ahmed body simplifies the shape of many cars. Bideaux *et al.* (2011), Gilliéron & Kourta (2013) have achieved 20% drag reduction for this configuration in an experiment. High-frequency blowing was applied orthogonal to the upper corner of the slanted rear surface. Intriguingly, the maximum drag reduction was achieved in a narrow range of frequencies and actuation velocities and its effect rapidly deteriorated for slightly changed parameters. In addition, the actuation is neither Coanda blowing nor an ideal candidate for shear-layer energization as the authors noted.

The manuscript is organized as follows. The employed optimization algorithm is first introduced. Then, the configuration and the numerical methods of the three benchmarks fol-

low. The optimized control commands and the resulted flow fields are analyzed hereafter. Finally, The outlook is given in the conclusion.

METHODOLOGY

This study employs the explorative gradient method (EGM) (Li *et al.*, 2022) as the optimizer for the active flow control with multiple parameters. This approach alternates between downhill simplex method (DSM) as a robust gradient method and Latin hypercube sampling (LHS) as the most explorative step. The pusedocode is described as algorithm 1. First, $N_D + 1$ vertices are initialized as the set S for the DSM operation, after which the S is updated by the best $N_D + 1$ parameters discovered so far. Here, N_D is the dimension of the parameter vector $\boldsymbol{b}$. Then, one sample $\boldsymbol{x_L}$ from the samples by LHS is selected to test, which is the furthest away from all hitherto studied data points. If $\boldsymbol{b}_L$ is better than any of the simplex vertices, it will replace the worst vertex to formulated the new simplex set S. The best vertex $\boldsymbol{b}^*$ is selected from the latest simplex vertices when the maximum iteration is met.

Algorithm 1: Explorative gradient method

Data: f, Ω, N_D, N_i

Result: $\mathbf{b}^* = \arg\min_{\mathbf{b} \in \Omega} f(\mathbf{b})$

$D, S, Y_D, Y_S \leftarrow InitSamples(f, \Omega, N_D + 1)$

while *iter* $\leq N_i$ **do**

$\quad S, Y_S = DSM(f, S)$

$\quad D, Y_D \leftarrow S, Y_S$

$\quad L = LHS(D)$

$\quad \boldsymbol{b}_L = \arg\max_{\boldsymbol{b}_i \in L} \min_{\boldsymbol{b}_i \in L, \boldsymbol{b}_j \in D} \left\| \boldsymbol{b}_i - \boldsymbol{b}_j \right\|.$

$\quad D, Y_D \leftarrow \boldsymbol{b}_L, f(\boldsymbol{b}_L)$

$\quad S = sort(Y_S, f(\boldsymbol{b}_L), N_D + 1)$

end

$\mathbf{b}^* = \arg\min_{\mathbf{b} \in S} Y_S$

CONFIGURATIONS & NUMERICAL SETUPS

The optimization goal in this study is to find the global minimum of the aerodynamic performance target J defined for different configurations in the design parameter space Ω of the control input $\boldsymbol{b}$

$$\boldsymbol{b}^\star = \arg\min_{\boldsymbol{b} \in \Omega} J(\boldsymbol{b}). \tag{1}$$

Fluidic pinball

The fluidic pinball (Deng *et al.*, 2020) is a benchmark configuration for wake control. It is geometrically simple yet rich in nonlinear dynamics behaviours. This configuration consists of a cluster of three equal, parallel and equidistantly spaced cylinders pointing in opposite to uniform flow (figure 1a). The wake can be controlled by the cylinder rotation. This study advance the complexity by adding one more columns with another three cylinders (figure 1b). The actuation commands b_i corresponds to the rotation velocities U_i, where the positive value denotes the anti-clockwise direction.

Following Cornejo Maceda *et al.* (2021), we aim to minimize of the averaged parasitic drag power $\bar{J}_a$ penalizing the averaged actuation power $\bar{J}_b$. The resulting cost function reads

$$\bar{J} = \bar{J}_a + \bar{J}_b. \tag{2}$$

The first contribution $\bar{J}_a = c_D$ corresponds to drag coefficient. Here, $\bar{F}_D$ denotes total averaged drag force on all cylinders per unit spanwise length. The second contribution arises from the necessary actuation torque to overcome the skin-friction resistance. In the subsequent study, the actuation commands are bounded by 5, i.e, the search space reads

$$\Omega := \{ \boldsymbol{b} \in \mathscr{R}^N : b_i \in [-5,5] \quad \text{for} \quad i = 1, \ldots, N \}. \tag{3}$$

where N is equal to 3 in figure 1a and equal to 6 in figure 1b.

An in-house implicit finite-element method solver 'UNS3' is employed. It is of third-order accuracy in space and time. The unstructured grids in figure contain 4225 triangles (8633 vertices) and 4901 triangles (11063 vertices) separately. This resolution is sufficient for up to 2 percent error in drag, lift and Strouhal number.

Ahmed body

The drag reduction of a 1:3-scaled Ahmed body is also studied. The model is characterized by a slanted edge angle of $\alpha = 35°$. Five groups of steady blowing slot actuators are deployed on all edges of the rear window and the vertical base, see figure 11 in Li *et al.* (2022). The drag coefficient, $J = c_D$, is computed by RANS (Reynolds-Averaged Navier-Stokes simulations) with the varying steady blowing as the control input. The 10-dimensional designed actuation space $\boldsymbol{b}$ includes amplitudes U_i and directions θ_i, $i = 1, \ldots, 5$. The former five parameters are capped by the incoming velocity, and the latter by $\pi/2$.

$$\Omega := \left\{ \boldsymbol{b} \in \mathscr{R}^{10} : \begin{array}{ll} b_i \in [0,2] & \text{for } i = 1, \ldots, 5 \\ b_i \in [-35/90, 1] & \text{for } i = 6 \\ b_i \in [-1, 1] & \text{for } i = 7, \ldots, 10 \end{array} \right\}. \tag{4}$$

The RANS simulations are based on the realizable $k - \varepsilon$ model. The spatial discretization is based on a second-order upwind scheme in the form of SIMPLE scheme based on a pressure-velocity coupling method. The simulations are performed with the commercial flow solver Ansys Fluent. The prediction of the uncontrolled and controlled cases is validated by the experiment and LES (Large eddy simulation).

RESULTS

The best control of the fluidic pinball is found after 78 evaluations:

$$\boldsymbol{b}^\star = (-0.08, 1.13, -1.15). \tag{5}$$

The cost function $J^\star = 1.3$ reveals a net drag power saving of 29% with respect to the unforced value $J_u = 1.8235$. This near-optimal actuation corresponds to 52% drag reduction, which requires 23% investment in actuation energy.

The optimization cost increases exponentially with the complexity added to the 6 cylinders configuration. It takes
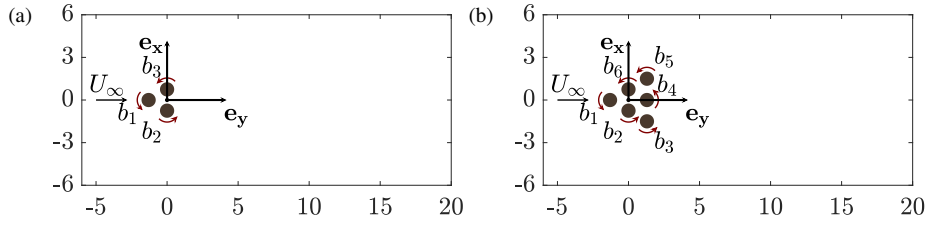
Figure 1: Fluidic pinball. (a) 3-cylinder configuration and (b) 6-cylinder configuration.

more than 400 evaluations to find the optimum $J = 2.457$ ($J_u = 2.8597$), 14% drag reduction, by the control command

$$\boldsymbol{b}^\star = (0.39, -0.15, 1.68, 0.05, -0.74, 0.09). \qquad (6)$$

Both the best actuation commands mimic nearly symmetric Coanda forcing with a circumferential velocity of nearly 1 (figure 2). This actuation deflects the flow towards the positive x-axis and effectively removes the dead-water region with reversal flow. The slight asymmetry of the actuation is not a bug but a feature of the optimal actuation after the pitchfork bifurcation at $Re_2 \approx 68$. This achieved performance and actuation is similar to the optimization feedback control achieved by machine learning control (Cornejo Maceda *et al.*, 2019), comprising a slightly asymmetric Coanda actuation with small phasor control from the front cylinder. Also, the optimized experimental stabilization of the high-Reynolds number regime lead to asymmetric steady actuation (Raibaudo *et al.*, 2020). The asymmetric forcing may be linked to the fact that the unstable asymmetric steady Navier-Stokes solutions have a lower drag than the unstable symmetric solution.

Top	Upper side	Middle	Lower side	Bottom
$b_1 = 0.8611$	$b_2 = 0.9856$	$b_3 = 0.0726$	$b_4 = 1.0089$	$b_5 = 0.8981$
$\theta_1 = -27°$	$\theta_2 = -42°$	$\theta_3 = 67°$	$\theta_4 = -44°$	$\theta_5 = 22°$

Table 1: Optimized actuation of the Ahmed body

The optimal actuation command for the Ahmed body found by EGM (see table 1) leads to 17% drag reduction ($c_D = 0.2586$) compared with the unforced flow ($c_D = 0.3134$). It takes only 354 RANS evaluations by the subspace-aided strategy. All peripheral actuators are directed inward. The top and bottom jets have inclinations of 27° and 22°, respectively, while side jets feature stronger inward angles of 42° and 44°, respectively. Intriguingly, the additional drag reduction by inward deflection of the jet-slot actuators has also been observed for the square-back Ahmed body (Barros *et al.*, 2016). Improved drag reduction with inward as opposed to tangential blowing was also observed for the 25° high-drag Ahmed body (Zhang *et al.*, 2018) and the square back version (Schmidt *et al.*, 2015). However, this is the first time the additive effects by the actuation direction is found on the slanted low-drag Ahmed body.
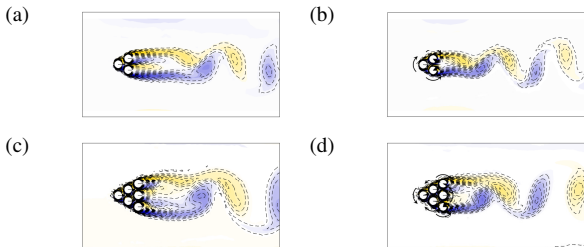
Figure 3 shows the streamwise velocity component and streamlines of the transversal velocity in the same plane for the unforced and actuated cases. The subfigures colorcode the pressure coefficient (left) as well as streamwise (middle) and vertical velocity components (right). The solid circle marks the furthest downstream extend of the dead-water region $(x,z)_{\text{DW}} = \arg\max_x \{u(x,0,z) \leq 0\}$. The squares denote in-plane velocity equilibrium associated with the vortices. The optimized flow is associated with an increase of the recirculation bubble and a more symmetric wake.

The more the wake is elongated the smaller the pressure gradient. A larger pressure in the near wake is related to the lower drag of the bluff body. This is confirmed by the pressure coefficient contours of figure 3 (left). Such correlation between length of the recirculation bubble and drag reduction has also been reported in actuated cylinder wakes (Gerhard *et al.*, 2003; Thiria *et al.*, 2006). Moreover, the wake becomes more slender and symmetric as featured by the velocity equilibrium points marking the vortex centers (solid squares). The increased up-down symmetry is facilitated by the upward blowing of the bottom jet. This peripheral inward blowing enables aerodynamic boat-tailing (Geropp, 1995) as new evidently more effective drag reduction mechanism. Similar observation is also reported on the square-back Ahmed body (Barros *et al.*, 2016; Haffner *et al.*, 2020), and a 25-degree Ahmed body Rossitto *et al.* (2016).

CONCLUSION

This paper reports an application study of the newly proposed optimizer — explorative gradient method (EGM). Three configurations with increasingly complex design space are included. Owing to the advantage of EGM over non-convex optimization problems, all the optimal solutions are targeted only at $O(100)$ simulations.

The net drag reduction of fluidic pinball with a 3- and 6-dimensional control space study foreshadows the benefit of the boat tailing solution by Coanda forcing. Finally, this strategy turns out to be the optimal drag reduction solution in a 10-dimensional design space composed of the steady blowing actuation for 35° Ahmed body.

EGM is not only an efficient but also a versatile optimizer framework with various future applications. In addition to parameter optimization, EGM can also be applied to model-free control law optimization, hitherto performed by genetic programming (Gautier *et al.*, 2015; Ren *et al.*, 2020) and deep reinforcement learning (Rabault *et al.*, 2019; Bucci *et al.*, 2019).

Figure 2: The unforced and optimally controlled wakes of 3-cylinder (a, b) and 6-cylinder (c, d) fluidic pinball.
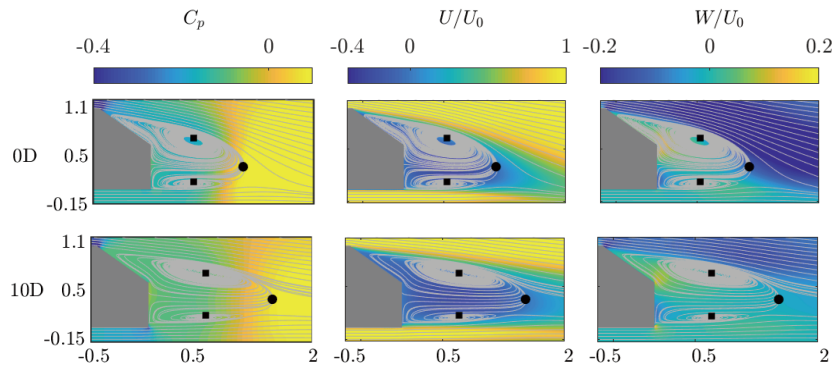
Figure 3: Flow visualization of the unforced and optimally controlled Ahmed body wakes in the symmetry plane $y = 0$.

REFERENCES

Barros, D., Borée, J., Noack, B. R., Spohn, A. & Ruiz, T. 2016 Bluff body drag manipulation using pulsed jets and Coanda effect. *J. Fluid Mech.* **805**, 442–459.

Bideaux, E., Bobillier, P., Fournier, E., Gilliéron, P., El Hajem, M., Champagne, J.-Y., Gilotte, P. & Kourta, A. 2011 Drag reduction by pulsed jets on strongly unstructured wake: towards the square back control. *Int. J. Aerodyn.* **1** (3-4), 282–298.

Blanchard, A. & Sapsis, T. 2021 Bayesian optimization with output-weighted optimal sampling. *J. Comput. Phys* **425**, 109901.

Bucci, M. A., Semeraro, O., Allauzen, A., Wisniewski, G., Cordier, L. & Mathelin, L. 2019 Control of chaotic systems by deep reinforcement learning. *Proc. Roy. Soc. London A* **475**, 20190351.

Cornejo Maceda, G. Y., Li, Y., Lusseyran, F., Morzyński, M. & Noack, B. R. 2021 Stabilization of the fluidic pinball with gradient-based machine learning control. *J. Fluid Mech.* **917**, A42:1–43.

Cornejo Maceda, G. Y., Noack, B. R., Lusseyran, F., Deng, N., Pastur, L. & Morzyński, M. 2019 Artificial intelligence control applied to drag reduction of the fluidic pinball. *Proc. Appl. Math. Mech.* **19** (1), e201900268:1–2.

Deng, N., Noack, B. R., Morzyński, M. & Pastur, L. R. 2020 Low-order model for successive bifurcations of the fluidic pinball. *J. Fluid Mech.* **884**, A37:1–39.

Gautier, N., Aider, J.-L., Duriez, T., Noack, B. R., Segond, M. & Abel, M. W. 2015 Closed-loop separation control using machine learning. *J. Fluid Mech.* **770**, 424–441.

Gerhard, J., Pastoor, M., King, R., Noack, B. R., Dillmann, A., Morzyński, M. & Tadmor, G. 2003 Model-based control of vortex shedding using low-dimensional Galerkin models. In *33rd AIAA Fluids Conference and Exhibit*, p. 4262.

Geropp, D. 1995 Process and device for reducing the drag in the rear region of a vehicle, for example, a road or rail vehicle or the like. United States Patent **US 5407245 A**.

Gilliéron, P. & Kourta, A. 2013 Aerodynamic drag control by pulsed jets on simplified car geometry. *Exp. Fluids* **54** (2), 1457.

Glezer, A., Amitay, M. & Honohan, A. M. 2005 Aspects of low- and high-frequency actuation for aerodynamic flow control. *AIAA Journal* **43** (7), 1501–1511.

Haffner, Y., Borée, J., Spohn, A. & Castelain, T. 2020 Unsteady coanda effect and drag reduction for a turbulent wake. *J. Fluid Mech.* **899**, A36:1–47.

Ishar, R., Kaiser, E., Morzynski, M., Albers, M., Meysonnat, P., Schröder, W. & Noack, B. R. 2019 Metric for attractor overlap. *J. Fluid Mech.* **874**, 720–752.

Li, Y., Cui, W., Jia, Q., Li, Q., Yang, Z., Morzyński, M. & Noack, B. R. 2022 Explorative gradient method for active drag reduction of the fluidic pinball and slanted ahmed body. *J. Fluid Mech.* **932**, A7.

Protas, B. 2004 Linear feedback stabilization of laminar vortex shedding based on a point vortex model. *Phys. Fluids* **16** (12), 4473–4488.

Rabault, J., Kuchta, M., Jensen, A., Réglade, U. & Cerardi, N. 2019 Artificial neural networks trained through deep reinforcement learning discover control strategies for active flow control. *J. Fluid Mech.* **865**, 281–302.

Raibaudo, C., Zhong, P., Noack, B. R. & Martinuzzi, R. J. 2020 Machine learning strategies applied to the control of a fluidic pinball. *Phys. Fluids* **32**, 015108:1–13.

Ren, F., Hu, H. & Tang, H. 2020 Active flow control using machine learning: A brief review. *J. Hydrodyn.* **32** (2), 247–253.

Reumschüssel, J., von Saldern, J., Li, Y., Paschereit, C. & Orchini, A. 2022 Gradient-free optimization in thermoacoustics: application to a low-order model. *J. Eng. Gas Turbine Power* **144** (5), 051004.

Rossitto, G., Sicot, C., Ferrand, V., Borée, J. & Harambat, F. 2016 Influence of afterbody rounding on the pressure distribution over a fastback vehicle. *Exp. Fluids* **57**, 1–12.

Schmidt, H.-J., Woszidlo, R., Nayeri, C. N. & Paschereit, C. O. 2015 The effect of flow control on the wake dynamics of a rectangular bluff body in ground proximity. *Exp. Fluids* **56**, 151.

Thiria, B., Goujon-Durand, S. & Wesfreid, J. E. 2006 The wake of a cylinder performing rotary oscillations. *J. Fluid Mech.* **560**, 123–147.

Wood, C. J. 1964 The effect of base bleed on a periodic wake. *Aeronaut. J.* **68** (643), 477–482.

Zhang, B. F., Liu, K., Zhou, Y., To, S. & Tu, J. Y. 2018 Active drag reduction of a high-drag Ahmed body based on steady blowing. *J. Fluid Mech.* **856**, 351—-396.